Classical and quantum phase-space behavior of a spin-boson system

Lothar Müller* and Joachim Stolze
Institut für Physik, Universität Dortmund, Postfach 500 500, W-4600 Dortmund 50, Germany

Hajo Leschke and Peter Nagel†
Institut für Theoretische Physik, Universität Erlangen-Nürnberg, Staudtstrasse 7, W-8520 Erlangen, Germany

(Received 21 December 1990)

We study the phase-space behavior of the standard two-level system (spin $\frac{1}{2}$) coupled to a harmonic oscillator (without the rotating-wave approximation), the classical counterpart of which is known to display deterministic chaos. We study the quantum-mechanical phase-space behavior by means of harmonic-oscillator coherent states (Husimi representation). Stationary quantum Poincaré sections may be defined; they show many parallels to their classical counterparts. We also study the time development of initially coherent states and observe a tendency towards a decay into many small wave packets in phase space for parameters in the chaotic regime.

I. INTRODUCTION

Various aspects of the correspondence between classical and quantum systems have been the subject of intense interest during the past 15 years or so, following the rapid development of nonlinear classical dynamics. The status of the quantum chaos problem has been reviewed several times.[1–4] Despite the large amount of effort devoted to the question, how the occurrence of classical chaos manifests itself in the properties of a corresponding quantum system, the answer is still far from clear. Thus, it is still worthwhile to study in detail the quantum-classical correspondence for simple model systems such as the one to be introduced below. Model studies of this kind have often concentrated on aspects of the energy spectrum (level statistics) or on the shape of energy eigenfunctions in coordinate representation, and important insights have been obtained in this way. However, as the notion of classical deterministic chaos is firmly based in phase space, it should be rewarding to construct suitable phase-space representations for quantum systems in order to detect similarities or differences to classical phase-space behavior. This type of approach was indeed followed by various authors in recent years.[5–14]

Beautiful studies of this kind were carried out by Chang and Shi,[8] and by Radons and Prange,[9] who compared quantum quasienergy eigenstates to classical Poincaré plots for a kicked rotator and obtained striking similarities. In the present paper, we shall report results of a similar study on a comparably simple, but autonomous system.

The system is defined by the quantum Hamiltonian

$$H=\tfrac{1}{2}(P^2+Q^2-1)+\omega_0 S_z+\sqrt{8}gQS_x \ . \tag{1}$$

P and Q are momentum and position operators of a single Cartesian degree of freedom, S_α ($\alpha=x,y,z$) are spin-$\frac{1}{2}$ operators. The operators obey the usual commutation relations, in particular,

$$PQ-QP=-i \quad (\hbar\equiv 1) \ ,$$
$$S_zS_x-S_xS_z=iS_y \ ,$$
$$\mathbf{S}^2\equiv S_x^2+S_y^2+S_z^2=\tfrac{3}{4} \ . \tag{2}$$

The Hamiltonian (1) describes a two-state system interacting with a harmonic oscillator, the natural frequency of which we use as a unit of energy; ω_0 is the level splitting of the unperturbed two-state system and g is the coupling parameter. For some purposes it is convenient to use a slightly different form of H, introducing raising and lowering operators for the spin $\frac{1}{2}$ and the oscillator in the usual way:

$$H=b^\dagger b+\omega_0 S_z+g(b+b^\dagger)(S_++S_-) \ . \tag{1'}$$

The model (1) enjoys great popularity in various fields of physics, such as atomic, molecular, and solid-state physics, and quantum optics. In its different fields of application, the Hamiltonian (1) bears different names, among them "Rabi Hamiltonian" and also "molecular polaron model"; references to earlier work may be found, for example, in Ref. 15.

Within the context of nonlinear dynamics and chaos, the model (1) probably was first studied by Belobrov, Zaslavski, and Tartakovski.[16] These authors considered a classical version of (1) and observed exponentially separating phase-space trajectories. Feinberg and Ranninger[17] used Poincaré plots to analyze the nonlinear behavior (of the classical model) in more detail. Graham and Höhnerbach[15] studied the dynamics of the quantum model and found that for sufficiently strong coupling the occupation probabilities of the two levels ($S_z=\pm\frac{1}{2}$) show irregular behavior, more precisely, they are quasiperiodic, involving a large number of incommensurate frequencies. For small coupling, the system behaves rather regularly and the occupation probabilities show periodic "revivals." The dynamics of analogous quantities in the classical model was studied in Refs. 18–20; chaotic be-

havior showed up on all these studies. On the other hand, numerical studies[21,22] of the eigenvalues of the quantum model revealed spectral features quite untypical for a system displaying quantum chaos: the nearest-neighbor level spacing distribution shows neither the Wigner behavior believed to be typical for chaotic systems nor the exponential form normally associated with integrable systems. Furthermore the spectrum shows striking regularities which can be described by an asymptotic scaling law for the highly excited states.[23] Graham and Höhnerbach[24] pointed out that the level-spacing distribution approaches the Wigner form if the single two-level system in (1) is replaced by N two-level systems (for example, $N=9$). In contrast to the one-spin model, the N-spin model has the advantage of possessing a well-defined classical limit.[15,25] Thus, studies of the N-spin model with varying N should be helpful in bridging the gap between the extreme quantum limit defined by (1) and its classical counterpart, and in observing the transition from quantal to classical dynamics.

In order to study the dynamics of the quantum model (1) in the usual arena of classical dynamics, that is, in phase space, Klenner, Doucha, and Weis[7] investigated the time dependence of the Wigner function defined on the bosonic phase space. However, the Wigner function has some disadvantages; it often shows violent oscillations between positive and negative values (on a scale given by Planck's constant) instead of vanishing in regions where the corresponding classical phase-space probability density is small. It is thus hard to decide whether the irregular time evolution observed in Ref. 7 is an indication of quantum chaos or merely an artifact of the Wigner function. In order to avoid these difficulties, we shall employ the Husimi phase-space density (see Ref. 26 and references cited there). This density is based on boson coherent states and equivalent to the "normal-ordered phase-space quasiprobability distribution"[27(a)] employed in quantum optics. The Husimi density is non-negative, because it eliminates the physically irrelevant $\hbar$-scale oscillations of the Wigner function by a minimal Gaussian smoothing[27(b)] in accordance with the minimum uncertainty property of the coherent states. In this sense the Husimi density represents the quantum state (pure or mixed) in phase space "as classically as possible."

Our paper is organized as follows. In Sec. II we present a classical counterpart of the model (1) and discuss some aspects of its phase-space behavior. We present some Poincaré plots and estimate the borderline in parameter space between regular behavior and large-scale chaos. In Secs. III and IV, respectively, we define stationary and dynamical "quantum Poincaré sections" based on the Husimi density and compare them to the classical Poincaré plots of Sec. II, in order to discuss aspects of the quantum chaos of the model (1). Finally, in Sec. V we summarize our results.

II. THE CLASSICAL CASE

As discussed by Graham and Höhnerbach,[15] there is more than one possibility to obtain a classical model from (1). We choose a classical analog which is given by the energy function

$$h=\tfrac{1}{2}(p^2+q^2)+\omega_0 s_z+\sqrt{8}gqs_x \ , \tag{3}$$

where q and p are the coordinate and momentum of a classical Cartesian degree of freedom, and $\mathbf{s}\equiv(s_x,s_y,s_z)$ is a classical vector. The dynamics is given by the (not fully canonical) equations of motion

$$\frac{dp}{dt}=-\frac{\partial h}{\partial q} \ , \quad \frac{dq}{dt}=\frac{\partial h}{\partial p} \ ,$$
$$\frac{d\mathbf{s}}{dt}=-\mathbf{s}\times\frac{\partial h}{\partial \mathbf{s}} \ , \tag{4}$$

which imply the conservation laws

$$\frac{dh}{dt}=0 \ , \quad \frac{d\mathbf{s}^2}{dt}=0 \ . \tag{5}$$

Writing the equations of motion more explicitly

$$\frac{dq}{dt}=p \ ,$$
$$\frac{dp}{dt}=-q-\sqrt{8}gs_x \ ,$$
$$\frac{ds_x}{dt}=-\omega_0 s_y \ , \tag{6}$$
$$\frac{ds_y}{dt}=\omega_0 s_x-\sqrt{8}gqs_z \ ,$$
$$\frac{ds_z}{dt}=\sqrt{8}gqs_y \ ,$$

we obtain five coupled nonlinear differential equations. Due to the two conservation laws (5), the effective state space has three dimensions, thus allowing for classical chaos. The classical model may be obtained from (1) in (at least) two ways. One may replace P and Q in (1) by the classical quantities p and q and the spin-$\frac{1}{2}$ operators by spin-S operators and then consider the limit $\hbar\to 0$, $S\to\infty$ with $\hbar S=$const, to obtain the energy function h (replacing $\hbar\mathbf{S}$ by the classical vector $\mathbf{s}$). (Strictly speaking, h is not a classical Hamiltonian, as it is not completely expressed in canonical variables; for a canonical formulation see, for example, Ref. 25.) Alternatively, one may write down the Heisenberg equations of motion corresponding to (1) and take expectation values, approximating expectation values of operator products by products of expectation values, to obtain the set of classical equations of motion (6). We note in passing that the "rotating-wave approximation" (RWA) popular in quantum optical applications of (1), that is, the neglect of $b^\dagger S_+$ and bS_- in (1′), makes the model exactly soluble in the quantum case[28] and integrable in the classical case (see, for example, Ref. 25). This is due to an additional conserved quantity ($b^\dagger b+S_z$ in the quantum notation) associated with the RWA.

The equations of motion (6) possess four stationary solutions or fixed points, the stability of which is governed by the parameters

$$\lambda\equiv\frac{\omega_0}{8g^2 s} \ , \quad \mu\equiv\frac{(1-\omega_0^2)^2}{32g^2\omega_0 s} \ , \tag{7}$$

where $s \equiv |\mathbf{s}|$. The first two fixed points are given by

$$p = s_y = 0 \ , \quad s_x = \pm s(1-\lambda^2)^{1/2} \ ,$$
$$q = -\sqrt{8} g s_z \ , \quad s_z = -s\lambda \ . \tag{8}$$

Obviously these fixed points exist only for $\lambda^2 < 1$; in this case they are the classical ground states (minimum energy configurations) and thus they are stable (elliptic) fixed points. The third and fourth fixed points are given by

$$q = p = s_x = s_y = 0 \ ,$$
$$s_z = -s\,\mathrm{sgn}(\omega_0) \quad \text{(FP3)} \ , \tag{9}$$
$$s_z = +s\,\mathrm{sgn}(\omega_0) \quad \text{(FP4)} \ .$$

These fixed points exist for all parameter values. FP3 is the ground state (and thus stable) for $\lambda^2 > 1$ and unstable for $\lambda^2 < 1$. FP4 is stable for $\mu^2 \geq 1$ and unstable otherwise.

The classical ground state and its energy e_0 are thus completely determined by the parameter λ. The classical ground-state energy is given by

$$e_0 = -|\omega_0| s [\tfrac{1}{2}(|\lambda|^{-1} + |\lambda|)\Theta(1-\lambda^2) + \Theta(\lambda^2 - 1)] \ , \tag{10}$$

where $\Theta(x)$ denotes the Heaviside unit-step function. Graphs of e_0 and the ground-state position of the oscillator are shown in Fig. 1. The bifurcation of the classical ground state at $\lambda^2 = 1$ was already discussed by Feinberg and Ranninger.[17] It is interesting to note that there exists a close analogy to the ground state of the quantum system, which is approximated very well by a superposition of two displaced oscillator ground states (that is, coherent states, which are minimum uncertainty states), as numerical evidence shows. (See Refs. 29 and 30 and also Sec. III below.)

We have studied the trajectories following from (6) for several parameter combinations by standard numerical integration procedures, for example, a fourth-order Runge-Kutta method. The occurrence of chaos or order in phase space is determined by the parameters λ and μ. For $|\lambda| \ll 1$ and $|\mu| \ll 1$ chaos invades almost the whole energetically available phase space. Regular structures may only be found close to the ground state(s). For $|\lambda| \gg 1$ and/or $|\mu| \gg 1$ the phase space exhibits mainly order, chaos may only occur in small regions close to the unstable fixed point(s).

We have defined a Poincaré surface of section by $s_y = 0$ with $(d/dt)s_y \leq 0$. [This corresponds to a minimum of $s_x(t)$, as may be seen from the equations of motion.] The most prominent features in the regular regions of our Poincaré plots are elliptic periodic points corresponding to stable periodic orbits of period $2k+1$["$(2k+1)$ resonances"], leading to "island chains" of $2k+1$ elliptic regions. Figure 2 shows a 7-resonance as an example. The parameter values chosen in the figure correspond to $\lambda = 4.2$ and $\mu = 16.48$ and thus phase space is expected to be predominantly ordered. However, as the energy is rather high, chaotic regions begin to show up, which originate from the hyperbolic periodic points situated between the elliptic ones, in accordance with the scenario of homoclinic chaos (see, for example, Ref. 31). The predominance of "odd resonances" in the classical system may be related to the paritylike symmetry of the quantum system

$$H\Pi = \Pi H \tag{11}$$

with

$$\Pi \equiv \exp[i\pi(b^\dagger b + S_z + \tfrac{1}{2})] \ . \tag{12}$$

This symmetry allows[15] for $(2k+1)$-quantum transitions associated with near degeneracies ("narrow avoided crossings") in the energy spectrum, especially for weak coupling (small g).

As discussed above, for small $|\lambda|$ there are two classical ground states, corresponding to stable equilibria of two symmetrically displaced harmonic oscillators. Poin-

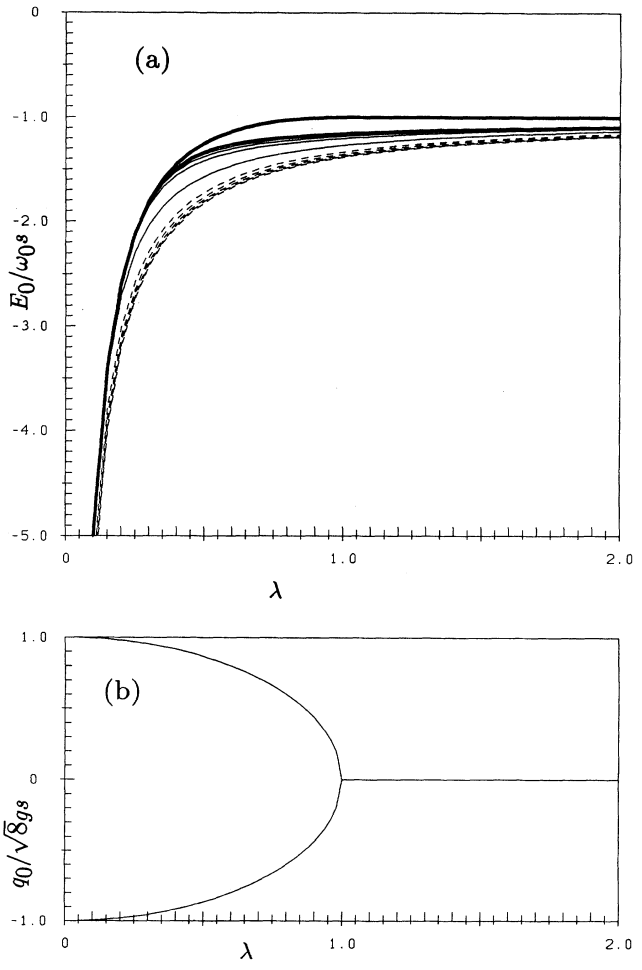

FIG. 1. (a) Classical and quantum ground-state energies in units of $\omega_0 s$, vs λ. The solid line represents the classical ground-state energy e_0 [Eq. (10)], the thin lines correspond to the quantum ground-state energy. The solid (dashed) lines correspond to the two possibilities in calculating g and ω_0 from given λ and μ [Eq. (7)]. The solid lines correspond to the larger g values, and to μ values of 0(0.4)2 (from bottom to top), whereas the dashed lines represent the smaller g values and the same series of μ values, from top to bottom. The dashed and solid lines for $\mu = 0$ coincide, as they should. (b) Classical equilibrium position of the oscillator, in units of $\sqrt{8}gs$, vs λ.

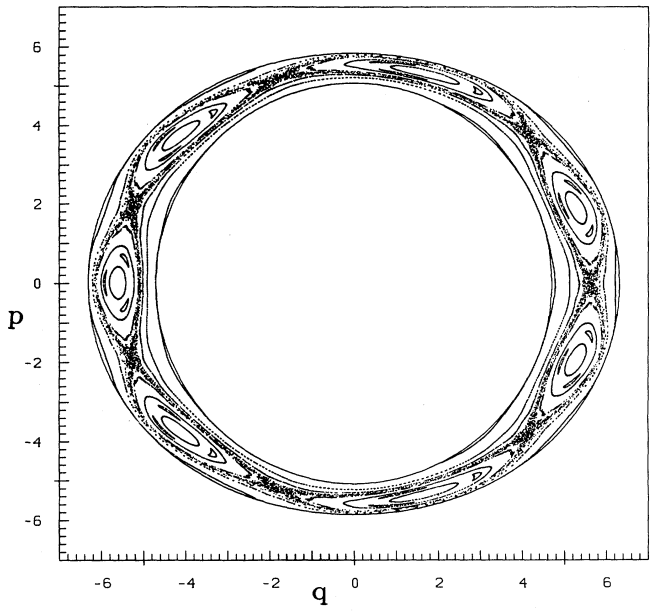

FIG. 2. Classical Poincaré plot of various trajectories for $g=0.5$, $\omega_0=4.2$, energy $h=15$. Abscissa is q, ordinate p.

caré plots at energies above the ground-state energy will then lead to large elliptic features encircling the ground states. These orbits, reflecting the symmetry of the displaced harmonic oscillator, are visible in many Poincaré plots, for example, in Figs. 3 and 4. For analogous features of the quantum system, compare Sec. III, especially Fig. 9.

We now turn to the interesting case of resonance, $\omega_0=1$, and strong coupling, $g=0.5$. In Figures 3–6 we observe a transition from integrability to global chaos with growing energy. At energy $h=-0.499$ (barely above the classical ground-state energy $e_0=-0.5$) the Poincaré plot shows already two elliptic fixed points, one in the center, and one close to the boundary of the allowed phase-space region. At $h=-0.48$ we observe a 3-resonance as a new structure, and for $h=-0.25$ a large variety of stable islands is observed, surrounded by a "chaotic sea" (Fig. 5). The transition to (almost) complete chaos (Fig. 6) is accompanied by a dominant 3-resonance (Fig. 5, C). Besides this dominant feature, Fig. 5 still shows the two fixed points (A,B) already observed at low energy, a 5-resonance (G), and small even reso-

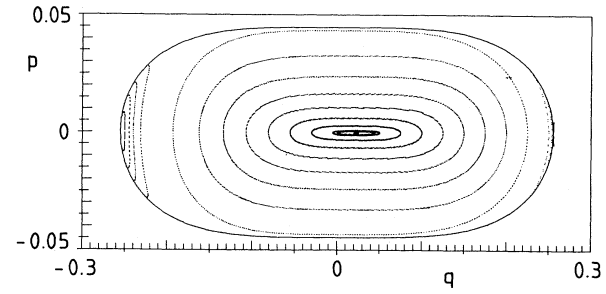

FIG. 3. Same as Fig. 2, for $g=0.5$, $\omega_0=1$, $h=-0.499$.

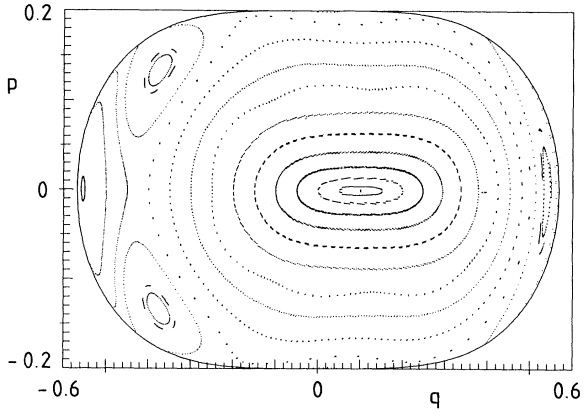

FIG. 4. Same as Fig. 3, for $h=-0.48$.

nances of period 4(F) and 6(H,I). Note that the 6-resonances are not symmetric with respect to the line $p=0$, in contrast to the remaining periodic points. In the following two sections we shall compare characteristic features of the classical Poincaré sections to corresponding quantum sections, which we shall introduce.

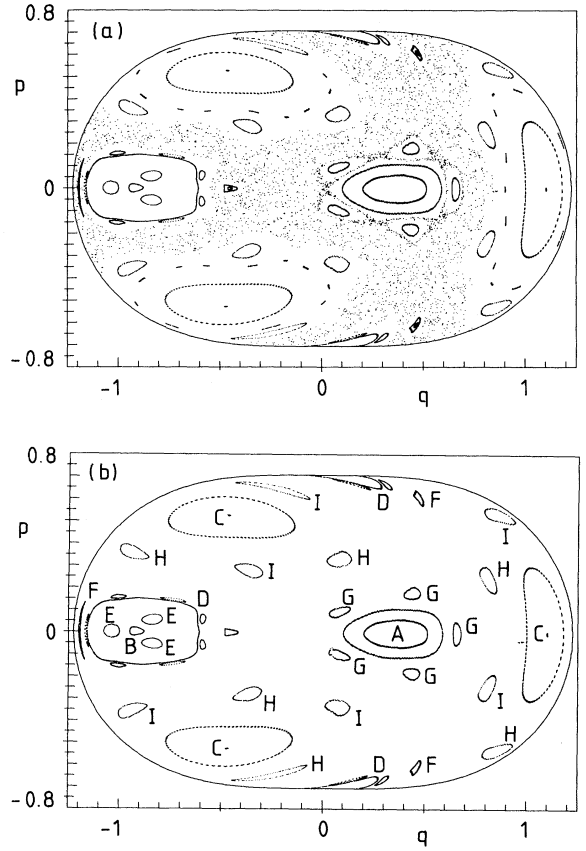

FIG. 5. (a) Same as Fig. 3, for $h=-0.25$. (b) Some of the regular structures of (a).

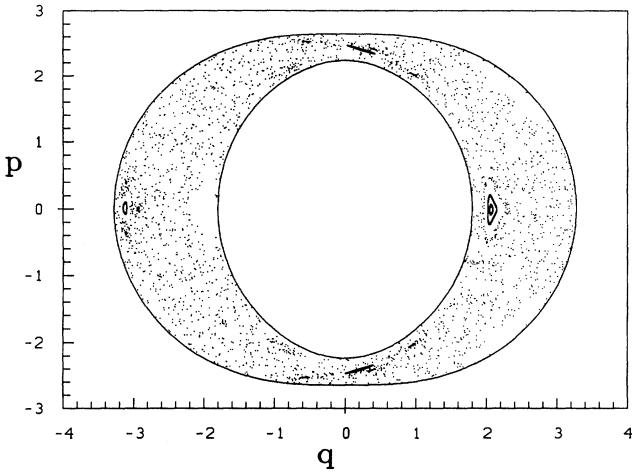

FIG. 6. Same as Fig. 3, for $h=3$. The chaotic "sea" of points is formed by one single trajectory.

III. STATIONARY QUANTUM POINCARÉ SECTIONS

In the present section we investigate the question whether any signature of the classical chaos shows up in the shape of the energy eigenstates of the quantal model (1). In the next section we shall consider the quantum dynamics. We define a phase-space description of the bosonic degree of freedom by means of the harmonic-oscillator coherent states:

$$|p,q\rangle \equiv \exp[i(pQ-qP)]|0\rangle \ , \tag{13}$$

where $|0\rangle$ is the ground state of a harmonic oscillator with unit mass and frequency [$\omega_0=g=0$ in (1)].

The unitary operator appearing in (13) describes a displacement of both position and momentum. It is thus clear that every coherent state may be associated with a phase-space point via

$$\langle p,q|Q|p,q\rangle = q \ , \quad \langle p,q|P|p,q\rangle = p \ . \tag{14}$$

From the oscillator ground state the coherent states inherit the property of minimum uncertainty product $\Delta p \Delta q$ and equal uncertainties $\Delta p = \Delta q$. Coherent states thus provide the closest possible quantum-mechanical analogs of classical phase-space points which makes them especially useful for studying the classical limit of quantum systems. (In fact, Schrödinger[32] introduced them for exactly this purpose.) The state $|p,q\rangle$ is an eigenstate of the annihilation operator $b \equiv (Q+iP)/\sqrt{2}$ with the complex eigenvalue

$$\alpha \equiv \frac{(q+ip)}{\sqrt{2}} \tag{15}$$

which is also often used to label the state. Due to the overcompleteness of the coherent states, operators are completely characterized by their diagonal elements in the coherent-state representation. A density operator $\rho=\rho^\dagger \geq 0$ may thus be described by the non-negative phase-space function

$$\rho(p,q) \equiv \langle p,q|\rho|p,q\rangle \tag{16}$$

which is called its Husimi density. For the special case of a pure state, $\rho=|\psi\rangle\langle\psi|$, the density $\rho(p,q)$ evidently reduces to $|\langle\psi|p,q\rangle|^2$. For more information on the properties of coherent states and of the Husimi density (especially as compared to the Wigner function), we refer the reader to Refs. 33, 34, and 26, respectively.

In order to compare stationary classical phase-space structures to corresponding features of stationary quantum states, one may try to construct quantum Poincaré sections. This is straightforward for purely bosonic systems: the phase space is introduced via (multi-mode) coherent states and a quantum Poincaré plot is defined as a contour plot of the Husimi density on the appropriate surface of section. In the study of nonlinear dynamical systems, this concept was first applied in Ref. 5. For the present spin-boson system the definition of a quantum Poincaré map is less evident. As the classical Poincaré surface of section was defined by the condition that $s_x(t)$ be minimum, we decided to use a projection to the negative x direction with respect to the quantum spin. We stress that this choice is to a certain extent arbitrary; there are several kinds of spin coherent states[33,34] which make other choices of the spin state possible.

We denote the eigenstates of H by $|N,\pm\rangle$, where $\pm$ denotes the "parity" Π [Eq. (12)], and $N=1,2,3,\ldots$. The ground state is $|1,+\rangle$. The eigenstates of S_x are denoted by $|\sigma\rangle$

$$S_x|\sigma\rangle = \sigma|\sigma\rangle \ , \quad \sigma = \pm\tfrac{1}{2} \tag{17}$$

and the product states

$$|\sigma,p,q\rangle \equiv |\sigma\rangle|p,q\rangle \tag{18}$$

serve to define the stationary Husimi density on the quantum Poincaré surface of section

$$w_{N,\pm}(p,q) \equiv |\langle N,\pm|-\tfrac{1}{2},p,q\rangle|^2 \ . \tag{19}$$

The numerical determination of the eigenstates $|N,\pm\rangle$ and the corresponding eigenvalues poses no particular problems. In a basis formed by simultaneous eigenstates of S_z, $b^\dagger b$, and Π (12), H is obviously given by a tridiagonal matrix. Eigenvalues and eigenvectors of the (suitably truncated) Hamiltonian matrix were determined by Sturmian bisection and inverse iteration.[35]

In analogy to the discussion of Sec. II, we first present our results on the quantum ground state. It is obvious from Eqs. (7) that for a given spin quantum number S ($S=\frac{1}{2}$ in our case) the parameters g and ω_0 are not uniquely determined by the values of λ and μ. In the classical case the ground-state energy (divided by $|\omega_0|$) and the oscillator ground-state position do not depend on the sign chosen in inverting (7). This is no longer true in the quantum case; furthermore, the ground-state properties now also depend on the parameter μ, in contrast to the classical case. Figure 1 shows results for the ground-state energy $E_{1,+}$ as a function of λ, for various values of μ. The differences between classical and quantum

ground-state energies are not large, nor does the quantum ground state depend strongly on μ or on the sign choice mentioned above.

We have studied the shape of the quantum ground state in phase space, that is, the function $w_{1,+}(p,q)$ (19) for values of λ between 0.1 and 2, and various values of μ, in order to look for the quantum-mechanical counterpart of the classical bifurcation at $\lambda=1$ shown in Fig. 1(b). Again we have to take into account that for given values of λ and μ, two sets of values of g and ω_0 are possible. Choosing the branch with larger g values leads to a ground state which clearly displays a bifurcation, whereas the ground state corresponding to the weak-coupling branch does not show spectacular changes of shape as λ and μ are varied. In the following we shall restrict our attention to the strong-coupling branch, if not explicitly stated otherwise. For $\lambda=2$, the Husimi density of the ground state on the quantum Poincaré surface of section displays a single maximum resembling the ground state of an unperturbed harmonic oscillator in its circularly symmetric Gaussian shape. For very large values of μ the contour lines of $w_{1,+}(p,q)$ change from circular to slightly elliptic shape. At $\lambda=1$ (where the bifurcation occurs in the classical system) the contour lines change from circular to pear shaped as μ grows, and for even larger μ, a slight constriction in the outermost contour lines begins to develop, signaling that a second maximum is about to appear. [It is often useful to study the logarithm of $w_{1,+}(p,q)$ in order to see emerging new structures.] This tendency becomes more obvious at $\lambda=0.5$; and at $\lambda=0.1$, the quantum ground-state picture in phase space is clearly dominated by two centers corresponding to the classical oscillator ground-state positions. In Fig. 7 we display $w_{1,+}(p,q)$ for $\lambda=0.1$, $\mu=10$ on a logarithmic scale. On a linear scale, the secondary maximum would hardly be visible, as it is about two orders of magnitude smaller than the absolute maximum. (There are, however, also parameter values for which the secondary maximum is clearly visible also on a linear scale, for example, $g=2.8$, $\omega_0=10$.)

For $\lambda=0.1=\mu^{-1}$ we have also computed the stationary quantum Poincaré sections of some excited states (up to $N=80$), and again the results are reminiscent of two symmetrically displaced oscillators: $w_{N,+}(p,q)$ is of appreciable size on two annuli of radius (approximately) $\sqrt{2N}$, centered around the classical oscillator ground-state positions. [Remember that for a harmonic oscillator eigenstate $|n\rangle$ the Husimi density is

$$|\langle n|\alpha\rangle|^2=|\alpha|^{2n}\frac{\exp(-|\alpha|^2)}{n!}\ , \tag{20}$$

which assumes its maximum value at $|\alpha|^2=(p^2+q^2)/2=n$.] Figure 8 shows the excited state $N=80$ as an example.

In order to study another interesting analogy between classical and quantum Poincaré plots, we consider the spectrum of H. In Fig. 9 we display some (positive-parity) energy levels as functions of ω_0, for fixed $g=0.5$. The presence of a large number of regularly arranged narrow avoided crossings of energy levels is a conspicuous (and well-known) property of the spectrum. The ar-

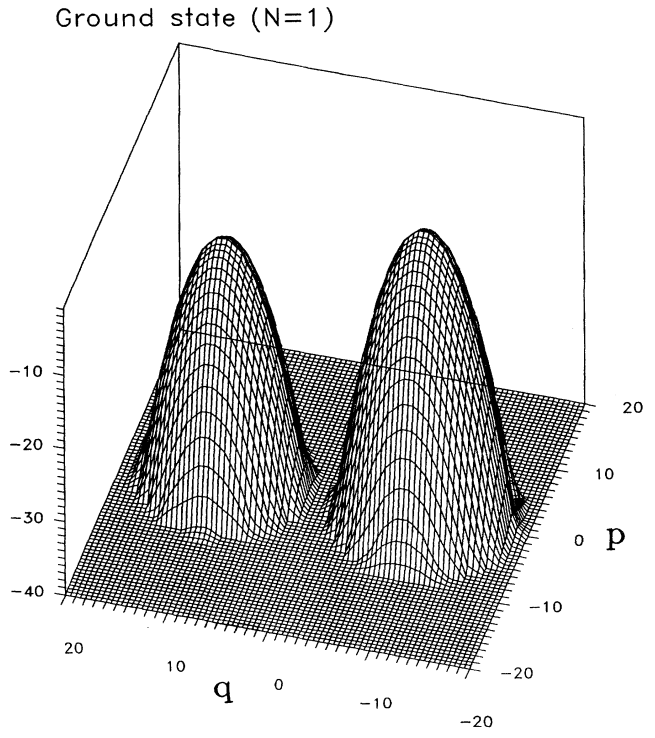

FIG. 7. Logarithm of the Husimi density $w_{1,+}(p,q)$ of the ground state, on the quantum Poincaré surface of section. Parameter values are $g=7.0799$, $\omega_0=20.05$ ($\lambda=0.1=\mu^{-1}$). Values of $w_{1,+}(p,q)$ less than e^{-40} have been omitted for clarity. The maxima are located at the ground-state positions of the corresponding classical oscillator, the maximum value of $w_{1,+}(p,q)$ is approximately 0.46.

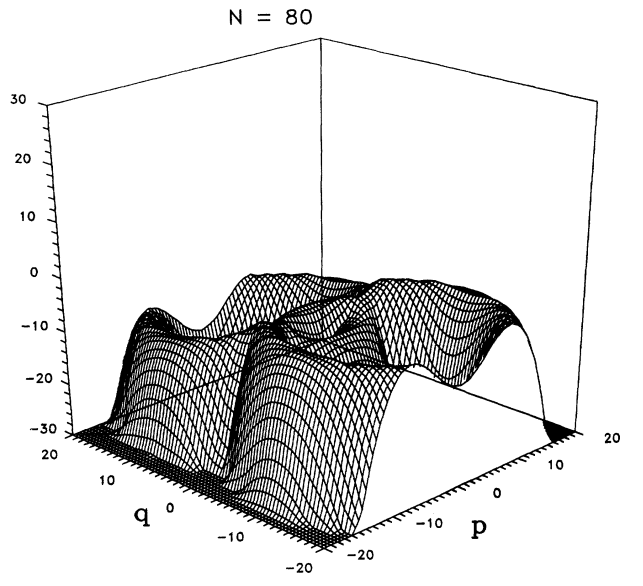

FIG. 8. Similar to Fig. 7, logarithm of $w_{80,+}(p,q)$. Values less than e^{-30} have been omitted.

rangement of these avoided crossings may be easily understood by considering the limit of zero coupling constant g. In this limit the spectrum of positive-parity eigenvalues is trivially given by

$$E_{N,+}=N-1+(-1)^N\frac{\omega_0}{2}\ . \tag{21}$$

The corresponding eigenstates are products of oscillator eigenstates (with quantum number $n=N-1$) and eigenstates of S_z [with eigenvalue $(-1)^N/2$]. For $\omega_0=2k+1$ ($k=0,1,\ldots$) the energies of the states with $N=2l$ ($l=1,2,\ldots$) and $N=2l+2k+1$ coincide, so that in a plot analogous to Fig. 9 we would observe strictly vertical "columns" of level crossings. For nonzero (but small) values of the coupling constant g, all these degeneracies are lifted and the resulting avoided crossings are shifted to other values of ω_0. This leads to the "distorted columns" of avoided crossings visible in Fig. 9. (The avoided crossings corresponding to $k=0$ and $k=1$ only appear for g values much smaller than 0.5 and thus are absent in Fig. 9.) It is reasonable to assume that the character of the two states involved in a given avoided crossing is not changed grossly, as compared to the zero-coupling case.

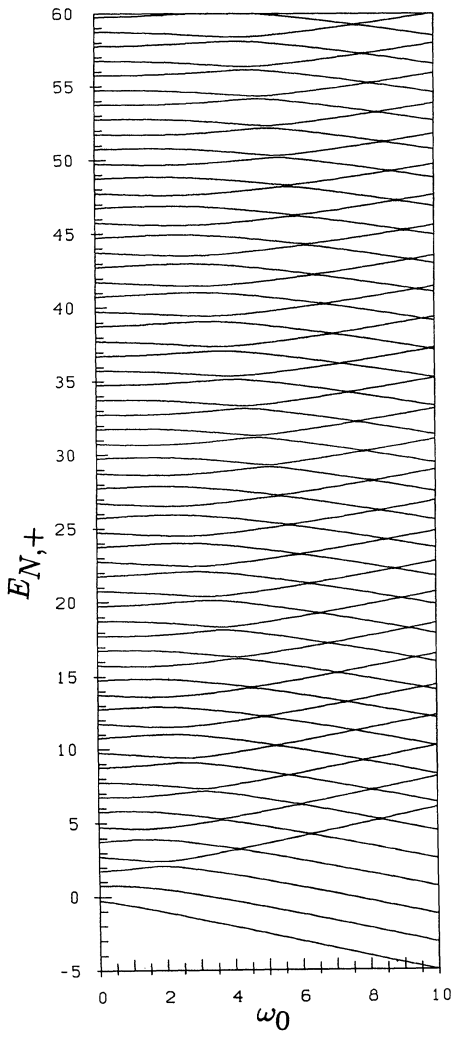

FIG. 9. Spectrum of positive-parity energy eigenvalues for $g=0.5$, and ω_0 between 0 and 10. All apparent level crossings are actually avoided.

Thus, in every avoided crossing of a given column, we may expect a pair of states closely related to the harmonic-oscillator states with quantum numbers $n=2l-1$ and $n=2(l+k)$. A superposition of these states leads to a characteristic shape in phase space. The Husimi densities of the two individual states yield circularly symmetric shapes [compare Eq. (20)]; however, there is also an "interference term" proportional to $\cos(2k+1)\phi$, where ϕ is a polar angle in the (p,q) plane. The resulting quantum phase-space picture with a $(2k+1)$-fold rotational symmetry will thus be characteristic for all avoided crossings of a given column. Of course, the eigenstates will tend to spread out more and more in phase space, as energy grows. In fact, this behavior is precisely what one finds numerically, and moreover, the classical phase-space structure as revealed by classical Poincaré plots shows striking parallels. We have studied this correspondence in some detail for $g=0.5$ and $\omega=4.2$. For these parameter values, the spectrum displays a series of narrow avoided crossings involving the pairs of states $(N,N+1)=(4,5),(17,18),(34,35),(59,60),(88,89)(119,120)$. As was to be expected from the $(2k+1)$-fold rotational symmetry of the zero-coupling states discussed above, the stationary quantum Poincaré plots of states involved in these avoided crossings show $2k+1$ maxima ($k=2,\ldots,7$) arranged around the origin in a roughly circular fashion. In contrast, states far away from avoided crossings (for example, $N=10$) do not show any pronounced phase-space structure. (A more or less trivial feature of any stationary quantum Poincaré plot at the present parameter values is the fact that the phase-space density is essentially concentrated on an annular region corresponding to the classical energy shell.) As an example of a state involved in an avoided crossing we show (in Fig. 10) a contour plot of the Husimi density (19) for the eigenstate $|18,+\rangle$. This figure should be compared to the classical Poincaré plot of Fig. 2, which corresponds to the same values of the coupling parameters, but to a slightly different energy. (The classical and quantum energy values of Figs. 2 and 10 are $h=15$ and $E_{18,+}=16.32$, respectively, where the corresponding ground-state energies are $e_0=-2.1$ and $E_{1,+}=-2.15$. A classical Poincaré plot at $h=16.37$, corresponding to the quantum eigenvalue $E_{18,+}$, does not differ from Fig. 2 in a qualitative way, nor are the phase-space structures displaced by any appreciable amount.) Figures 2 and 10 are both dominated by a cycle of seven phase-space "islands" coinciding very well. Of course, small-scale structures in classical Poincaré plots are invisible in quantum Poincaré plots due to the uncertainty relation $\Delta p\,\Delta q\geq\frac{1}{2}$.

As discussed above, every avoided crossing is related to its zero-coupling counterpart involving two harmonic-oscillator eigenstates. In the avoided crossing involving the state of Fig. 10 we thus expect the oscillator states

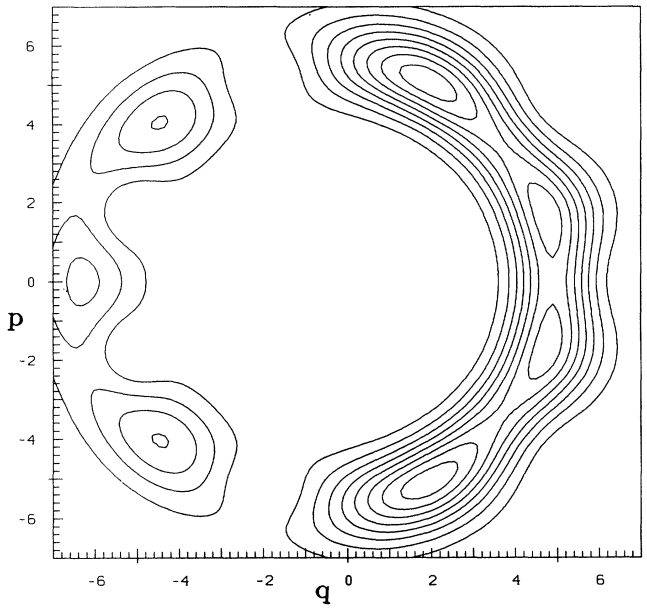

FIG. 10. Contour plot of a stationary quantum Poincaré section at $g=0.5$, $\omega_0=4.2$, eigenstate $|18,+\rangle$. This picture should be compared to the classical Poincaré plot in Fig. 2.

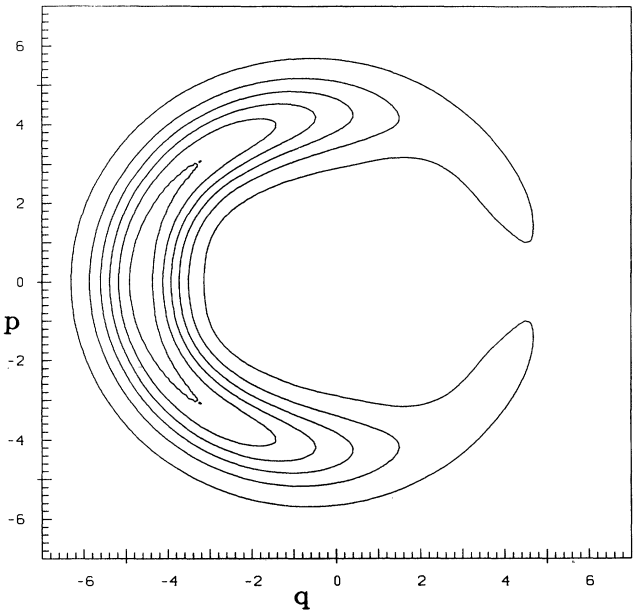

FIG. 11. Same as Fig. 10, eigenstate $|8,+\rangle$.

$n=13$ and $n=20$ to dominate, and this is confirmed by the numerical results. The two oscillator states contribute roughly two-thirds to each of the two eigenstates with $N=17$ and 18, respectively, i.e.,

$$|\langle n=13,\sigma=+\tfrac{1}{2}|N=18,\Pi=+1\rangle|^2 + |\langle n=20,\sigma=-\tfrac{1}{2}|N=18,\Pi=+1\rangle|^2\approx\tfrac{2}{3}$$

and similarly for $N=17$. If ω_0 is changed so that one moves away from the avoided crossing, one of the two dominant eigenvector components becomes stronger and the other one weaker. Thus the interference effect leading to the observed approximate $(2k+1)$-fold rotational symmetry becomes weaker and the observed phase-space structure gets lost. A similar loss of structure occurs if a pair of states immediately above or below an avoided crossing is considered, e.g., the two states $N=19$ and 20 at $\omega_0=4.2$. Of course, these two states are also involved in an avoided crossing, which, however, occurs at a different value of ω_0 and thus the interference effect mentioned above does not fully show up. States far away from any avoided crossing do not show any significant nontrivial phase-space structure. As a typical example we show the state $|8,+\rangle$ in Fig. 11.

As exemplified in Figs. 2 and 10, the classical Poincaré plots show the same kind of symmetry as the corresponding quantum Poincaré plots. However, the change of symmetry with increasing energy (at constant ω_0) occurs in a different way. In contrast to the quantum Poincaré plot, the classical Poincaré plot does not completely lose its structure at an energy value halfway between two neighboring avoided crossings. Instead, as energy increases ,the $2k+1$ islands dominating the Poincaré plot at a given avoided crossing move inward and at the outer boundary of the energetically allowed phase-space region a new set of $2k+3$ islands appears which is going to dominate at the next higher avoided crossing. The two sets of regular island structures are separated by a chaotic layer which tends to become wider as energy grows.

It would be interesting to look into quantum phase-space behavior in more detail in order to see whether the small-scale classical structures have quantum counterparts, and whether individual quantum states related to stable and unstable classical periodic orbits may be identified, as Radons and Prange[9] recently demonstrated in the case of the kicked rotator. For this purpose, however, the effective value of Planck's constant must be changed, i.e., higher spin quantum numbers must be studied.

At resonance ($\omega_0=1$, and strong coupling, $g=0.5$) the correspondence between classical and quantum Poincaré plots is not as close as in the case discussed above ($\omega_0=4.2$, $g=0.5$). In the present case, the parameters λ and μ (7) are unity and zero, respectively, so we expect classical chaos to be far more pronounced than in the former case, where both λ and μ were fairly large. Whereas the classical Poincaré plot shows almost complete chaos already at energy $h=3$ (Fig. 6) with small stable period-3 islands, quantum Poincaré plots at comparable energies, for example, for the states $N=4$ (Fig. 12) and $N=5$ show rather clear features of threefold rotational symmetry whose extent in phase space is much larger than that of the classical islands in Fig. 6. At higher energies, classical chaos invades the whole available phase-space region, whereas stationary quantum Poincaré plots still show some degree of regular structure, for example, approximate fivefold or sevenfold symmetries close to the states $N=12$ (Fig. 13) and $N=24$, respectively. It should be noted that these symmetries of the quantum Poincaré plots may again be traced back to

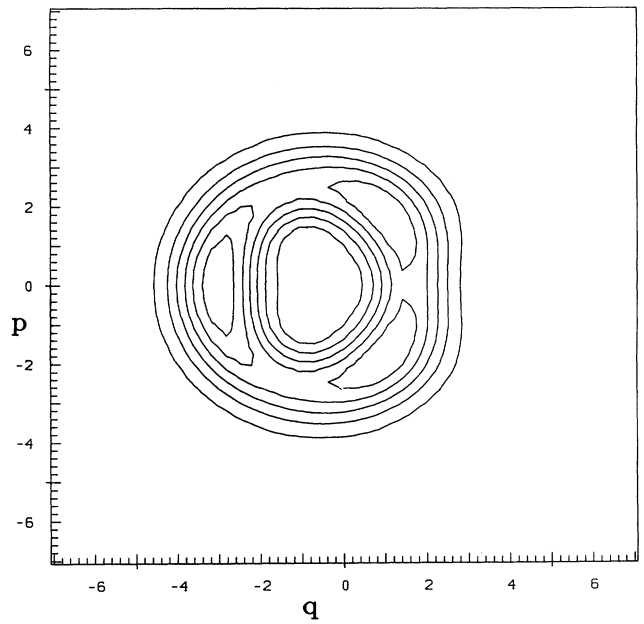

FIG. 12. Same as Fig. 10, for $g=0.5$, $\omega_0=1$, eigenstate $|4,+\rangle$.

nearby avoided crossings in the energy spectrum (Fig. 9), as in the case of $\omega_0=4.2$.

We have confirmed these observations by also looking at the behavior for $g=0.5$, $\omega_0=1.8$, where the avoided crossings are more clearly visible than for $\omega_0=1$. The lowest avoided crossing occurs between states $N=3$ and 4. It is associated with a quantum Poincaré plot of approximate threefold rotational symmetry, as it should be. The corresponding classical Poincaré plot shows small islands sets of the same symmetry in a sea of chaos. The next higher avoided crossing occurs at $N=14,15$, and the quantum Poincaré plot shows the expected fivefold symmetry, whereas the classical Poincaré plot shows complete chaos. It thus seems that quantum-mechanical phase-space structure is more robust toward chaos than classical phase-space structure. Again, a study at higher spin quantum numbers should be able to shed some light on this question.

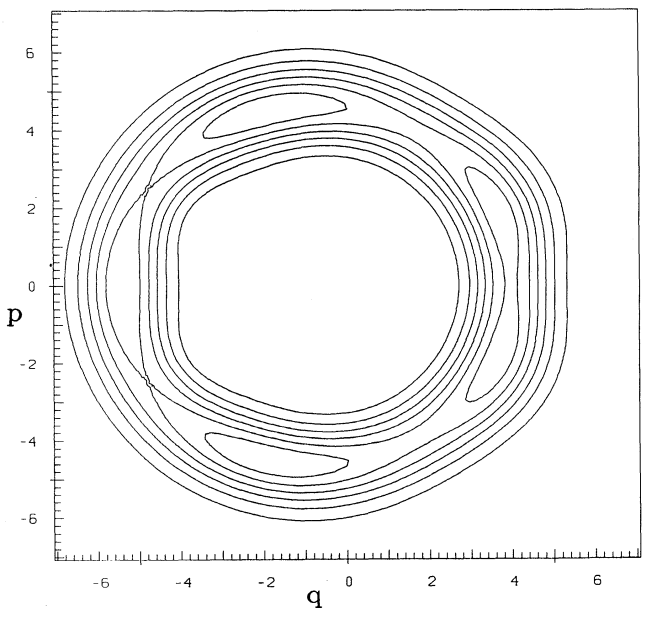

FIG. 13. Same as Fig. 12, eigenstate $|12,+\rangle$.

IV. DYNAMICAL QUANTUM POINCARÉ SECTIONS

In order to study quantum dynamics in phase space, we define the Husimi matrix of a time-dependent state vector $|\psi(t)\rangle$ of the full quantum system as follows:

$$w_{\sigma,\sigma'}(p,q,t)\equiv\langle\sigma,p,q|\psi(t)\rangle\langle\psi(t)|\sigma',p,q\rangle\ . \tag{22}$$

Its trace

$$w(p,q,t)\equiv\sum_{\sigma}w_{\sigma,\sigma}(p,q,t) \tag{23}$$

completely characterizes the (reduced) state of the bosonic subsystem, whereas the full matrix (22) contains the full information on $|\psi(t)\rangle$. We shall consider the time evolution of initial states of the form

$$|\psi(0)\rangle=|\tfrac{1}{2},p_0,q_0\rangle \tag{24}$$

for different p_0,q_0. The quantum analog of a point in a classical Poincaré map then is a snapshot of $w(p,q,t_p)$, where the "Poincaré time" t_p is defined by the quantum analog

$$\langle S_y\rangle=0\ ,\quad \frac{d}{dt}\langle S_y\rangle\le 0 \tag{25}$$

of the classical Poincaré condition. (See Sec. II above.)

In the trivial case $g=0$, the phase-space density (23) corresponding to the initial state (24) is a simple two-dimensional Gaussian moving along the classical phase-space orbit of a harmonic oscillator with the period 2π and without changing its shape. For nonzero coupling the situation is, of course, different, and in the case of resonance and strong coupling ($\omega_0=1$, $g=0.5$) the initial boson coherent state is almost completely destroyed after one period. Let us discuss some typical pictures of $w(p,q,t_p)$. In Fig. 14 we have chosen $q_0=3/\sqrt{8}$, $p_0=0$, leading to a rather low energy expectation value ($\langle H\rangle=1.3125$; the ground-state energy is $E_{1,+}=-0.6333$). The phase-space density shows two maxima which one might associate with the classical periodic (elliptic) orbits shown in Fig. 3. (Note, however, that in Fig. 3, the energy is much closer to its ground-state value.) For $q_0=3/\sqrt{2}$, $p_0=0$ ($\langle H\rangle=3.75$) we observe a large variety of substructures (see Fig. 15). Summing up $w(p,q,t_p)$ for several consecutive values of t_p leads to some smoothing and the remaining structure consists of three maxima reminiscent of the dominant 3-resonance in the classical Poincaré plot of Fig. 5. A large amount of phase-space structure is observed at $q_0=5/\sqrt{2}$, $p_0=0$ ($\langle H\rangle=7.25$, Fig. 16): there are two kidney-shaped wave packets (M_1) and a roughly circular

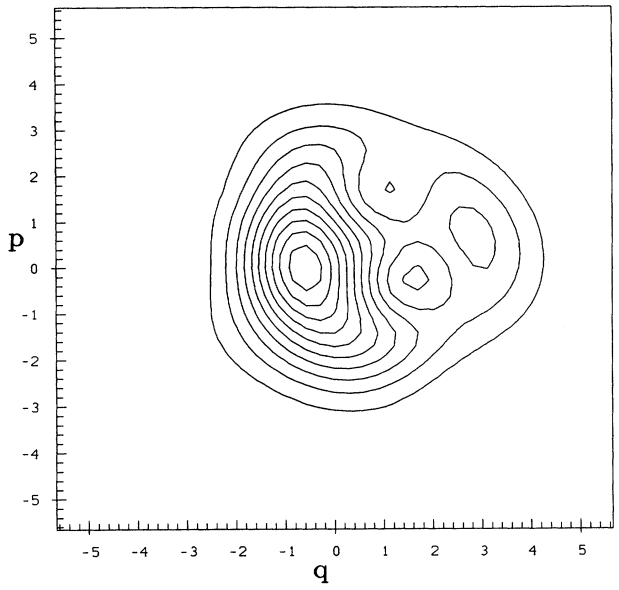

FIG. 14. Trace $w(p,q,t)$ of the Husimi matrix of an initially coherent state with $q_0=3/\sqrt{8}$, $p_0=0$, at the "Poincaré time" $t_p=7.64\pi$, in the case of resonance and strong coupling ($\omega_0=1, g=0.5$). The contour lines correspond to values of 0.05, 0.1, 0.15, etc.

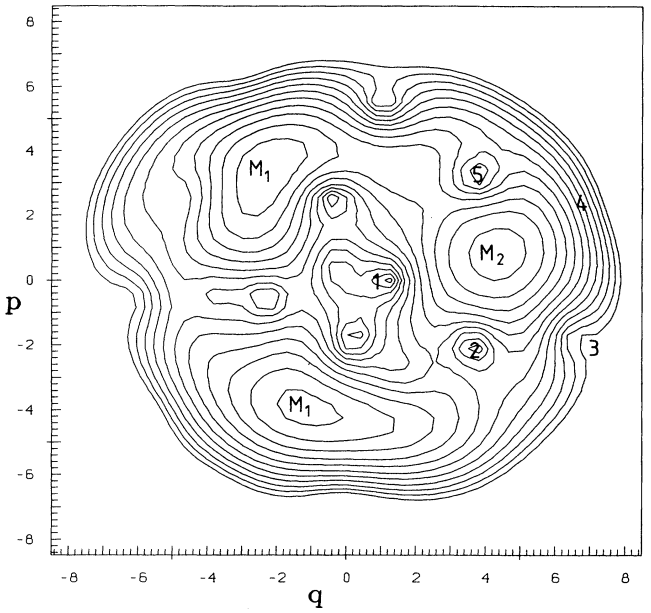

FIG. 16. Same as Fig. 14, for $q_0=5/\sqrt{2}$, $t_p=50.64\pi$, logarithmic. M_1 and M_2 denote the main maxima; at 1, 2, 3, and 5, there are minima. For reasons of symmetry, one would expect another minimum at 4.

one (M_2) which is surrounded by a (roughly) fivefold symmetric structure of ridges and valleys. This structure again resembles the classical phase-space structures displayed in Fig. 5 (compare especially the regions marked A and G). At still higher energy ($q_0=4\sqrt{2}$, $p_0=0$, $\langle H\rangle=20$, Fig. 17) the phase-space density splits up into many small wave packets which are rather evenly distributed over the energetically available phase-space region. No particular ordered phase-space structure is discernible.

To summarize, we can tentatively identify phase-space structures from classical Poincaré plots and quantum "Poincaré snapshots." Similar sequences of structures

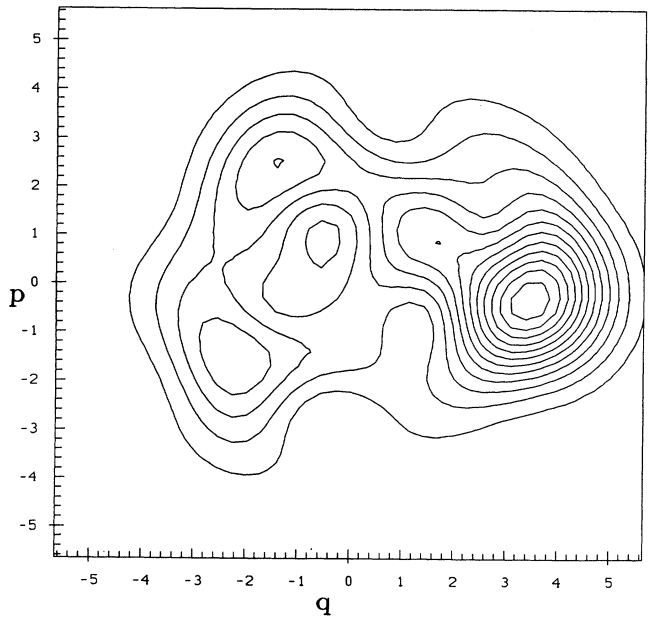

FIG. 15. Same as Fig. 14, for $q_0=5/\sqrt{2}$, $t_p=50.75\pi$. The contour lines correspond to values of 0.03, 0.06, etc.

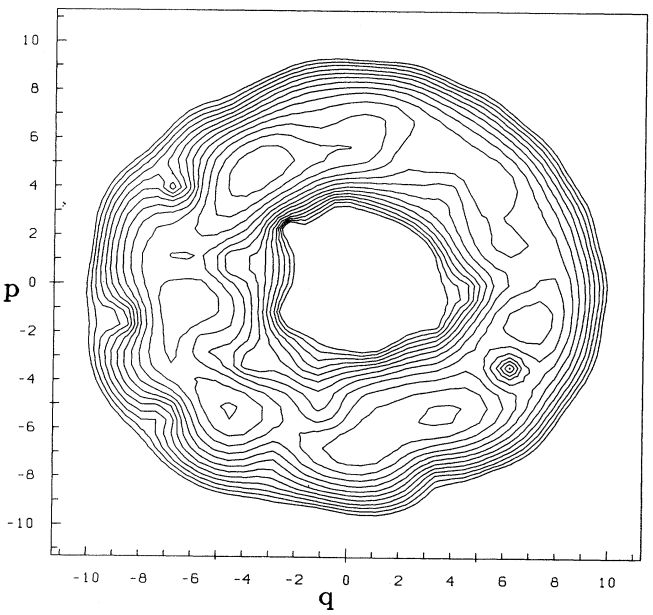

FIG. 17 Same as Fig. 14, for $q_0=8/\sqrt{2}$, $t_p=51.78\pi$, logarithmic.

develop in both cases as energy increases; the energy scales, however, are quite different.

V. SUMMARY AND OUTLOOK

We have studied the phase-space behavior of a simple two-state model coupled to a harmonic oscillator. A classical limit of this model is known to display chaotic behavior, whereas the quantum model may be called integrable in a certain sense. In the classical case we have found that the degree of chaos of the system may be simply characterized by the two parameters λ and μ (7). To study the quantum phase-space behavior we have employed the Husimi density based on harmonic-oscillator coherent states. The Husimi representation turns out to be ideally suited for the study of quantum phase-space phenomena as it does not mask intrinsic structures in phase space by spurious oscillations, in contrast to the Wigner function which is also often used for similar purposes. We have defined stationary quantum Poincaré sections corresponding to stationary states as well as dynamical quantum Poincaré maps reflecting the time development of the closest possible quantum approximation to a classical phase-space point, namely, an initially coherent state. Despite the apparent conflict between classical chaos and quantum integrability, we have observed many parallels between classical and quantum phase-space structures. In the regular part of parameter space we observe phase-space patterns dominated by tori (associated with displaced harmonic oscillator orbits) and "chains" of $2k+1$ islands (associated with stable periodic orbits). The island chains in the stationary quantum Poincaré plots may be understood in terms of the well-known narrow avoided crossings (near degeneracies) occurring in the energy spectrum for not too strong coupling. The quantum-mechanical phase-space patterns seem to be more stable against chaos than their classical counterparts. In dynamical quantum Poincaré "snapshots" we also have observed parallels to regular classical phase-space features, even for parameter values where the classical system shows completely chaotic behavior. If parameters are changed to an even more strongly chaotic regime, we observe a decay of an initially coherent state into many seemingly independent wave packets in phase space.

In the present (spin-$\frac{1}{2}$) model it is difficult to study in great detail the parallels between classical and quantum-mechanical phase-space behavior due to the limited resolution imposed by the uncertainty relation. A study at higher spin quantum numbers should be able to supply finer phase-space details. Employing coherent states for the spin as well as for the harmonic oscillator would give additional flexibility in defining alternative Poincaré surfaces of section which might provide further insight into the quantum dynamics. A more systematic study should also involve a comparison between the nature of the classical phase-space trajectories and the trajectories of the corresponding quantum-mechanical expectation values developing from an initially coherent state. A study of this kind was recently performed by Fox and Lan[36] for the kicked rotator. Another interesting topic is the role of dynamical barriers in quantum phase space, (i.e., tori and cantori) which has been studied for the kicked rotator in.[37] To summarize, we have found many interesting parallels between classical and quantum phase-space structures, but in contrast to Radons and Prange[37] we did not detect the quantum analogs of Kol'mogorov-Arnol'd-Moser tori and other small-scale classical phase-space structures in the present extreme quantum limit, $S=\frac{1}{2}$. Finer phase-space structures will probably show up at higher spin quantum numbers.

ACKNOWLEDGMENTS

We are grateful to Manfred Schmutz for many interesting discussions that helped initiate this project, to Werner Weber for generous computer support, and to Bernd Lamberts for advice on computer graphics. One of us (L.M.) acknowledges financial support by the Studienstiftung des Deutschen Volkes.

---

*Present address: Institut für Metallforschung, BH 18, Technische Universität Berlin, Strasse des 17 Juni 135, W-1000 Berlin 12, Germany.

†Present address: Lehrstuhl für Rechnergestützten Schaltungsentwurf, Universität Erlangen-Nürnberg, Wetterkreuz 13, W-8520 Erlangen, Germany.

[1] *Stochastic Behavior in Classical and Quantum Hamiltonian Systems,* edited by G. Casati and J. Ford, Lecture Notes in Physics Vol. 93 (Springer, Berlin, 1979).

[2] *Chaotic Behavior in Quantum Systems—Theory and Applications,* edited by G. Casati (Plenum, New York, 1985).

[3] *Quantum Measurement and Chaos,* edited by E. R. Pike and S. Sarkar (Plenum, New York, 1987).

[4] *Chaos and Quantum Physics,* Proceedings of the Summer School of Theoretical Physics, Les Houches, 1989, edited by A. Voros, M. J. Giannoni, and O. Bohigas (North-Holland, Amsterdam, 1990); a recent review article is B. Eckhardt, Phys. Rep. **163**, 205 (1988); two recent monographs are M. C. Gutzwiller, *Chaos in Classical and Quantum Mechanics* (Springer-Verlag, New York, 1990); F. Haake, *Quantum Signatures of Chaos* (Springer-Verlag, Berlin, 1991).

[5] Y. Weissman and J. Jortner, J. Chem. Phys. **77**, 1486 (1982).

[6] K. Takahashi and N. Saitô, Phys. Rev. Lett. **55**, 645 (1985).

[7] N. Klenner, M. Doucha, and J. Weis, J. Phys. A **19**, 3631 (1986).

[8] S.-J. Chang and K.-J. Shi, Phys. Rev. Lett. **55**, 269 (1985); Phys. Rev. A **34**, 7 (1986).

[9] G. Radons and R. E. Prange, Phys. Rev. Lett. **61**, 1691 (1988); see also G. Radons and R. E. Prange, in Proceedings of the Adriatico Research Conference on Quantum Chaos, Trieste, Italy, 1990 (to be published).

[10] M. Founargiotakis, S. C. Farantos, G. Contopoulos, and C. Polymilis, J. Chem. Phys. **91**, 1389 (1989).

[11] R. V. Jensen, M. M. Sanders, M. Saraceno, and B. Sundaram,

Phys. Rev. Lett. **63**, 2771 (1989).
[12]R. T. Skodje, H. W. Rohrs, and J. V. van Buskirk, Phys. Rev. A **40**, 2894 (1989).
[13]J. L. Anchell, J. Chem. Phys. **92**, 4342 (1990).
[14]P. Leboeuf and M. Saraceno, Phys. Rev. A **41**, 4614 (1990).
[15]R. Graham and M. Höhnerbach, Z. Phys. B **57**, 233 (1984).
[16]P. I. Belobrov, G.M. Zaslavski, and G. Kh. Tartakovski, Zh. Eskp. Teor. Fiz. **71**, 1799 (1976) [Sov. Phys.—JETP **44**, 945 (1976)].
[17]D. Feinberg and J. Ranninger, Physica D **14**, 29 (1984).
[18]P. W. Milonni, J. R. Ackerhalt, and H. W. Galbraith, Phys. Rev. Lett. **50**, 966 (1983).
[19]R. F. Fox and J. Eidson, Phys. Rev. A **34**, 482 (1986).
[20]N. Klenner, J. Weis, and M. Doucha, J. Phys. C **19**, 4673 (1986).
[21]M. Kuś, Phys. Rev. Lett. **54**, 1343 (1985).
[22]W. H. Steeb, C. M. Villet, and A. Kunick, Phys. Rev. A **32**, 1232 (1985).
[23]M. Schmutz, J. Phys. A **19**, 3565 (1986).
[24]R. Graham and M. Höhnerbach, Phys. Rev. Lett. **57**, 1378 (1986).
[25]R. Graham and M. Höhnerbach, in *Quantum Measurement and Chaos* (Ref. 3), p. 147.
[26]K. Takahashi, Prog. Theor. Phys. Suppl. **98**, 109 (1989).
[27](a) See, for example, W. H. Louisell, *Quantum Statistical Properties of Radiation* (Wiley, New York, 1973); or K. E. Cahill and R. J. Glauber, Phys. Rev. **177**, 1882 (1969). (These authors use the term "quasiprobability distribution.") (b) N. D. Cartwright, Physica A **83**, 210 (1976).
[28]E. T. Jaynes and F. W. Cummings, Proc. IEEE **51**, 126 (1963).
[29]H. B. Shore and L. M. Sander, Phys. Rev. B **7**, 4357 (1973).
[30]J. Stolze and L. Müller, Phys. Rev. B **42**, 6704 (1990).
[31]R. H. G. Helleman, *Fundamental Problems in Statistical Mechanics V,* edited by E. G. D. Cohen (North-Holland, Amsterdam, 1980), p. 165.
[32]E. Schrödinger, Die Naturwissenschaften **14**, 664 (1926).
[33]J. R. Klauder and B.-S. Skagerstam, *Coherent States—Applications in Physics and Mathematical Physics* (World Scientific, Singapore, 1985).
[34]A. Perelomov, *Generalized Coherent States and their Applications* (Springer, Berlin, 1986).
[35]J. H. Wilkinson, *The Algebraic Eigenvalue Problem* (Oxford University Press, London, 1968).
[36]R. F. Fox and B. L. Lan, Phys. Rev. A **41**, 2952 (1990).
[37]G. Radons, T. Geisel, and J. Rubner, Adv. Chem. Phys. **73**, 891 (1988); see also, T. Geisel, G. Radons, and J. Rubner, Phys. Rev. Lett. **57**, 2883 (1986).